Structure

An epitope-directed selection strategy facilitating the identification of Frizzled receptor selective antibodies

Graphical abstract

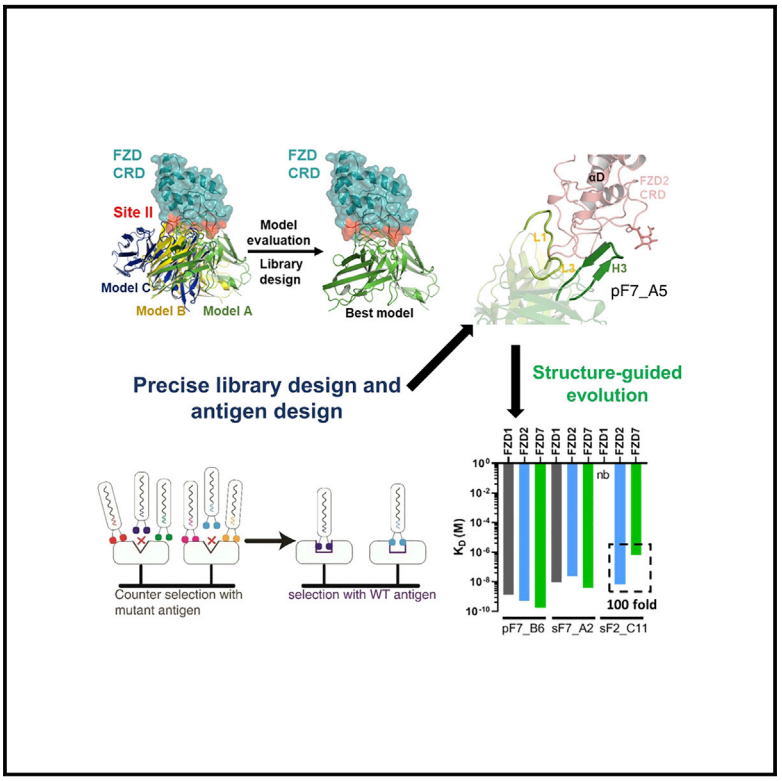

Highlights

- Epitope-directed antibody identification aided by library and antigen design
- An antibody targeting the desired Frizzled 2/7 site II region was identified
- Structure-guided evolution enables the identification of highly specific variants
- Epitope-specific antibodies show the expected modulations of the Wnt pathway

Authors

Qiangqiang Ge, Maikun Teng, Xu Li, Qiong Guo, Yuyong Tao

Correspondence

mkteng@ustc.edu.cn (M.T.),
sachem@ustc.edu.cn (X.L.),
qguo32@ustc.edu.cn (Q.G.),
taoyy@ustc.edu.cn (Y.T.)

In brief

The identification of antibodies with desired modulatory activities remains a challenging task. Ge et al. established a broadly applicable antibody isolation method that allows the selection of antibodies targeting specific regions on Frizzled receptors. The isolated antibodies showed the expected modulations of the Frizzled receptor-mediated signaling pathway.

Ge et al., 2023, Structure *31*, 33–43
January 5, 2023
https://doi.org/10.1016/j.str.2022.11.009

CellPress

Structure

CellPress

Article

An epitope-directed selection strategy facilitating the identification of Frizzled receptor selective antibodies

Qiangqiang Ge,[1] Maikun Teng,[2,*] Xu Li,[2,*] Qiong Guo,[1,*] and Yuyong Tao[1,3,4,*]
[1]Department of Clinical Laboratory, The First Affiliated Hospital of USTC, Ministry of Education Key Laboratory for Membraneless Organelles & Cellular Dynamics, Biomedical Sciences and Health Laboratory of Anhui Province, School of Life Sciences, Division of Life Sciences and Medicine, University of Science and Technology of China, 230027 Hefei, P.R. China
[2]Ministry of Education Key Laboratory for Membraneless Organelles & Cellular Dynamics, Biomedical Sciences and Health Laboratory of Anhui Province, School of Life Sciences, Division of Life Sciences and Medicine, University of Science and Technology of China, 230027 Hefei, P.R. China
[3]Joint Laboratory of Innovation in Life Sciences University of Science and Technology of China (USTC) and Changchun Zhuoyi Biological Co. Ltd., 130616 Changchun, P.R. China
[4]Lead contact
*Correspondence: mkteng@ustc.edu.cn (M.T.), sachem@ustc.edu.cn (X.L.), qguo32@ustc.edu.cn (Q.G.), taoyy@ustc.edu.cn (Y.T.)
https://doi.org/10.1016/j.str.2022.11.009

SUMMARY

The lack of incorporating epitope information into the selection process makes the conventional antibody screening method less effective in identifying antibodies with desired functions. Here, we developed an epitope-directed antibody selection method by designing a directed library favoring the target epitope and a precise "counter" antigen for clearing irrelevant binders in the library. With this method, we successfully isolated an antibody, pF7_A5, that targets the less conserved region on the FZD2/7 CRD as designed. Guided by the structure of pF7_A5-FZD2^{CRD}, a further round of evolution was conducted together with the "counter" antigen selection strategy, and ultimately, an FZD2-specific antibody and an FZD7-preferred antibody were obtained. Because of targeting the predefined functional site, all these antibodies exhibited the expected modulatory activity on the Wnt pathway. Together, the method developed here will be useful in antibody drug discovery, and the identified FZD antibodies will have clinical potential in FZD-related cancer therapy.

INTRODUCTION

Monoclonal antibodies are immunoglobulin molecules secreted by the immune system mainly to fight invading pathogens. Because of their exceptional properties, such as high binding affinity/specificity and engineerability, monoclonal antibodies have been widely used in biomedical studies as well as pharmacology.[1] Especially in recent years, immune checkpoint-blocking antibodies have achieved great success in cancer therapy.[2] Obviously, in the future, an increasing number of monoclonal antibodies will be explored as therapeutics for the treatment of a variety of diseases. Currently, three main methods are used for antibody identification: hybridoma technology, the phage display platform, and the recently developed single B cell sequencing.[3] For both hybridoma and single B cell technology, the first step is to immunize the experimental animals with the target antigens, which is often costly and time consuming.[4,5] After that, immunized B cells showing antigen-binding activity were recovered to generate antibodies with desired functions. In contrast, animal immunization can be skipped for the phage display platform, as pre-constructed naive libraries can be directly used for biopanning.[6,7] This feature makes phage display possess special advantages for raising antibodies in a very short period or against toxic antigens.[8]

Although high-affinity antibodies could be effectively identified with the above methods, these binders may not be suitable for further development into therapeutics, as therapeutic antibodies often need to recognize a functionally relevant epitope to elicit the desired outcome.[9] For example, targeting the interface within the ligand-receptor pair to obtain blocking antibodies and binding at the conserved patch across family members to generate pan-neutralizers. However, conventional approaches do not take epitope information into account during the selection process, and the binding affinity or accessibility/immunogenicity of the antigenic sites is often the only driving force for enriching the candidates.[10] As a result, candidates from these non-epitope-directed selections frequently need further detailed biochemical characterizations, and sometimes even no desired antibody could be resolved. To address this challenge, novel strategies have been developed. As a proof-of-concept study, antibody binding at a predefined epitope on interleukin-17A was successfully designed *in silico* on the basis of hundreds of

existing antibodies.[11] In addition to the computational method, an experimental approach using epitope-directed photocrosslinking was also developed.[12] In this method, the noncanonical amino acid p-benzoyl-l-phenylalanine (pBpa) was incorporated around the target epitope to covalently capture the phage displaying the required antibody. Although these methods demonstrated feasibility, they have drawbacks as well (e.g., losing the impact of affinity during the design or selection process and needing to prepare non-natural antigen derivatives). Therefore, developing alternative epitope-directed selection methods is still worthwhile.

The Wnt signaling pathway plays a key role in cell proliferation and the self-renewal of stem cells.[13] In humans, 10 frizzled (FZD) subtypes are the main receptors of the Wnt pathway, and their over-activation is tightly associated with cancers.[14,15] For example, FZD2 is generally overexpressed in cell lines derived from late-stage mesenchymal-type hepatocellular carcinomas (HCCs) and can regulate epithelial-mesenchymal transition as well as metastasis[16]; FZD5 maintains the growth of RNF43-mutant pancreatic ductal adenocarcinoma cells (PDACs)[17]; FZD7 is upregulated in hepatocellular carcinoma, colorectal cancer, and triple-negative breast cancer[18–21]; and FZD10 is linked to synovial sarcomas and colorectal cancers.[22,23] Although targeting FZDs with antibodies has significant therapeutic potential, there are great challenges, as the 10 FZDs share high sequence similarity and the sorted antibodies often yield cross-reactivity with the FZDs, resulting in undesired side effects.[24] Therefore, using discriminative epitopes on FZD receptors for the identification of selective antibodies to block or activate the cognate receptor involved in a specific physiological process is of great value. To this end, we developed an epitope-directed antibody identification method by including antigen design and library design, with which we successfully obtained FZD-selective antibodies.

RESULTS

Deriving FZD10 binder from a template antibody

The Wnt signaling pathway is initiated by Wnt binding to the extracellular cysteine-rich domain (CRD) of FZD receptors. The 10 FZD CRDs share almost identical fold and surface features, which are the key reason for the pleiotropic effects of Wnt ligands. The determined structure of Wnt-FZD8^{CRD} revealed that Wnt employs a "thumb finger" and an "index finger" to grasp the CRD domain through two distinct sites, named site I and site II.[25,26] Therefore, antibodies targeting CRD site I or site II to block Wnt binding yield inhibitory effects on the Wnt pathway.[27,28] Sequence conservation analysis revealed that the site I region is highly conserved among the FZD1/2/7 and FZD5/8 subfamilies but shows variations in other members, especially FZD9/10 (Figure S1A). As a result, a panel of FZD CRD antibodies recognizing site I could simultaneously bind FZD1/2/7, FZD5/8, and even FZD4, but not FZD9/10.[27,29] Despite not being sequence conserved, the surface shape of site I from FZD9/10 still shares similarity with those from FZD1/2/5/7/8 (Figure S1B), which prompted us to explore whether an FZD9/10 site I antibody could be easily derived from a pre-existing FZD1/2/5/7/8 site I binder (Figure S2A). As FZD10 is involved in synovial sarcomas and its specific antibody will have great therapeutic significance,[23] we chose FZD10 as the target for the first attempt.

To this aim, we thought screening FZD10 against a directed library constructed on the basis of an FZD1/2/4/5/7/8 antibody with known antigen-antibody interaction details would be the best method. Hence, we chose F2.I monoclonal antibody (mAb), as it targeted the FZD5 site I region, and its complex structure with FZD5 was also available.[28] We inspected the interface of F2.I-FZD5^{CRD} complex and randomized several relevant residues in the CDRs (Figure S2B). Specifically, those facing the antigen were randomized with full amino acid coverage to produce differentiated binding ability, but those inward-facing residues were kept to maintain the relative conformation (Figure S2B). The recombinant Fc-tagged FZD10 CRD was then used to select the phage library. After four rounds of biopanning, three positive colonies with unique sequences, named F10_A9/F10_E10/F10_H7, were discovered (Figure 1A). Interestingly, in addition to the shared FZD10 binding ability, these three antibodies presented varied specificity profiles for the other FZDs: F10_A9 could also bind FZD5/8, F10_E10 bound FZD9 as well, and F10_H7 was an exclusive FZD10 binder (Figure 1A).

To verify the binding epitope of these antibodies, we conducted crystallographic studies. The structure of the F10_A9-FZD10^{CRD} complex was determined at 2.65 Å resolution (Table 1). As expected, F10_A9 bound at the site I region of the FZD10 CRD, and the interaction surface was mediated mainly by the LCDR3 loop and HCDR3 loop (Figure 1B). Comparison of the F10_A9-FZD10^{CRD} structure with the template the F2.I-FZD5^{CRD} structure revealed that although F10_A9 and F2.I approach CRD with a slightly different angle; they both use LCDR3 and HCDR3 to engage the hydrophobic cleft spanning site I (Figure 1B). In addition, the complex structure also provided insights into the specificity of F10A_A9. E76 of FZD10 forms a salt bridge with R99 from HCDR3 (Figure 1C). The equivalent Glu in FZD5/8 probably fulfilled the same role (Figure 1C). However, the Lys or Gln substitution in FZD1/2/7 or FZD4/9 would disrupt this key electrostatic interaction, leading to loss of F10_A9 binding ability (Figure 1C). Interaction tests with the corresponding mutant FZDs again supported the structural observations: Glu-to-Lys mutation in FZD5/8/10 abolished its F10_A9 binding ability; meanwhile, K91E mutation in FZD7 and Q81E mutation in FZD9 conferred the F10_A9 binding activity (Figure S2C).

We also tried to solve the structure of FZD10^{CRD} complexed with F10_E10 and F10_H7. However, after many efforts, neither F10_E10 nor F10_H7 crystallized together with FZD10^{CRD}, even though they possessed an FZD10 binding affinity comparable with that of F10_A9 (Figures S2D and S2E). To continue deciphering the binding epitope of F10_E10 and F10_H7, we performed both competitive ELISAs and molecular docking analysis. As shown in Figure 1D, the presence of F10_E10 and F10_H7 greatly reduced the binding signal of F10_A9, demonstrating that their binding epitope overlaps with that of F10_A9, which is still the preset site I region. Consistently, the interaction sites revealed by the docking structures of F10_E10 and F10_H7 matched well with the binning assays (Figure S2F). Together, these results demonstrate that we can successfully identify antibodies binding to various antigens by screening a directed library constructed on the basis of a known "homolog" template.

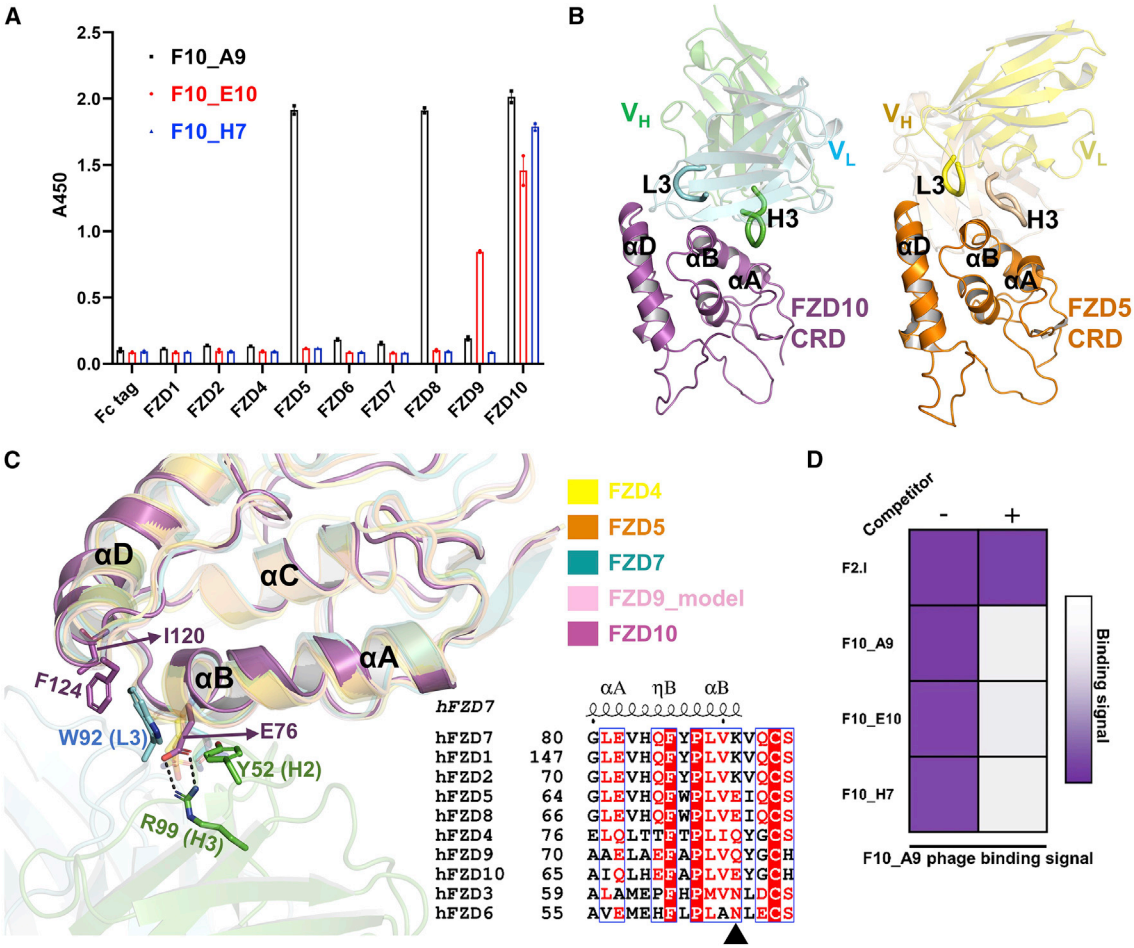

Figure 1. Identification and characterization of the FZD10 antibodies

(A) FZD binding specificity of the isolated antibodies. ELISA of the three anti-FZD10 IgGs (10 nM) on FZDs. Data are presented as mean ± SE of two replicates.

(B) Binding interface of F10_A9 on FZD10. The template antibody F2.I-FZD5^{CRD} complex (right) is viewed by aligning FZD5 with F10_A9-bound FZD10. LCDR3 and HCDR3 are labeled as L3 and H3, respectively.

(C) Structural and sequence comparison of the F10_A9 targeting region in different FZDs. The key residues involved in the specific interaction between F10_A9 and FZD10 are highlighted as sticks. The triangle indicates the position of E76.

(D) Epitope binning results of the FZD10 antibodies. The indicated IgGs (200 nM) were used to compete with FZD10_A9 phage for binding coated FZD10.

See also Figures S1 and S2.

FZD10-SPECIFIC ANTIBODY YIELDED BY TARGETING A NONCONSERVED EPITOPE

During the epitope binning assays of the above identified FZD10 antibodies, we used a known FZD10-specific antibody, B9L9.3.[30] Humanized B9L9.3 (hB9L9.3) showed strict FZD10 specificity and competed weakly with F10_A9 for binding to FZD10 (Figures S3A–S3C), which suggested that it may occupy an epitope exclusive to FZD10 but not fully overlapping with site I. Meanwhile, as hB9L9.3 can effectively inhibit the FZD10-mediated Wnt pathway, we thought hB9L9.3 might target a unique functional epitope on FZD10. To uncover where it engages, thus providing clues for designing other FZD-specific antibodies, we solved the structure of the FZD10 CRD bound with the Fab fragment of hB9L9.3 (Figure 2A) (Table 1). Surprisingly, hB9L9.3 recognizes a previously unreported epitope, the region located roughly on the opposite side of site II (Figure 2A). hB9L9.3 engagement did not affect the accessibility of site I or site II for Wnt ligand (Figure 2A). However, based on the models of the determined XWnt8-mFZD8^{CRD} and hWnt3-mFZD8^{CRD}, the V_H region of the bound hB9L9.3 seems to induce steric hindrance with the C-terminal subdomain of Wnt (Figure S3D), resulting in the blocking activity of hB9L9.3 on the Wnt pathway.

Analysis of the epitope recognized by hB9L9.3 revealed that it formed an "L"-shaped stretch hugged mainly by LCDR3, HCDR2, and HCDR3 of hB9L9.3 (Figure 2B). This epitope is the least conserved region in the FZD CRD, reflected by remarkable sequence divergences and conformational variations (Figure 2C). However, compared with the closest homolog FZD9, it still retains conservation, as of all the residues making contact with hB9L9.3, only four residues (R135/K136/N144/Y145) are FZD10 specific (Figure 2C). Interestingly, even with these few differences, hB9L9.3 can still discriminate FZD10 from FZD9/10 through the corresponding contacts conferred by the paratope

Table 1. Data collection and structure refinement statistics

	F10_A9-FZD10^{CRD}	hB9L9.3-FZD10^{CRD}	pF7_A5-FZD2^{CRD}
Data collection			
Wavelength (Å)	0.9792	0.9793	0.9792
Space group	$P4_12_12$	$P1$	$P1$
Cell dimensions			
a, *b*, *c* (Å)	156.45, 156.45, 94.29	75.46, 100.79, 99.15	66.38, 66.66, 90.91
α, β, γ (°)	90, 90, 90	110.08, 89.94, 113.79	95.14, 109.15, 115.33
Resolution (Å)[a]	50–2.65 (2.70–2.65)	50.00–2.50 (2.54–2.50)	27.76–2.24 (2.29–2.25)
Unique reflections	34,538 (1,698)	83,801 (4,163)	59,980 (2,991)
R_{merge} (%)	10.5 (87.8)	10.8 (34.5)	9.2 (49.3)
$I/\sigma(I)$	29.2 (3.8)	10.2 (3.3)	14.5 (2.9)
CC1/2	1.00 (0.90)	0.98 (0.90)	0.98 (0.82)
Completeness (%)	100.0 (100.0)	98.7 (98.0)	98.4 (96.1)
Redundancy	16.6 (16.9)	3.5 (3.3)	3.5 (3.1)
Refinement			
Resolution (Å)	36.88–2.65	46.06–2.51	27.76–2.24
R_{work}/R_{free} (%)	20.51/24.73	17.58/21.49	21.55/24.14
Number of atoms			
Protein	8270	16492	8334
Ligand			46
Water	177	1144	315
B factors (Å^2)			
Protein	50.49	38.47	36.4
Ligand			89.44
Water	37.83	40.54	36.47
RMSDs			
Bond lengths (Å)	0.007	0.012	0.007
Bond angles (°)	1.048	1.293	0.969
Ramachandran plot			
Favored (%)	97.09	97.12	96.8
Allowed (%)	2.91	2.88	3.2

RMSD, root-mean-square deviation.
[a]High-resolution shell is shown in parentheses.

(Figures 2B and 2C). Therefore, we conclude that by targeting the nonconserved epitope in CRDs, even showing few variations, highly selective antibodies could be generated.

Epitope-directed identification of FZD1/2/7 selective antibody

Comparison of the two key functional sites (site I and site II) in FZD CRDs clearly shows that site II is much less conserved than site I (Figure S4A), which means that the site II region could serve as the discriminative epitope for isolating antibodies with FZD subtype specificity. We then tried to explore a method to accomplish this site II-directed antibody identification, through which FZD-selective antibodies could be obtained. Inspired by the successful acquisition of antibodies possessing template-like epitopes using the above "homolog" library method (Figure S2A), we thought that redesigning from a site II antibody would fulfill the goal. However, no site II binder has been reported, so we next borrowed the idea used in the computational design of FZD binders, that is, docking the alanine model of an irreverent scaffold onto the target to obtain a desired complex model according to the surface shape complementarity.[31,32] To do this, we chose F2.I and hB9L9.3 as templates and trimmed the side chains of the CDR residues. As a proof-of-concept study, we chose the FZD1/2/7 subfamily as the target antigens because they show similarity as well as differences in the site II region (Figure S4B), facilitating further specificity tunability study (see below). Moreover, FZD1/2/7 over-activation has been linked to several cancers[16,19]; therefore, their specific antibodies will have clinical significance. To dock the antibody, site II was set as the contact site to remove unwanted docking results. When docked with hB9L9.3, FZD2/7 was repeatedly observed to adopt one highly similar interaction mode with hB9L9.3, suggesting that this mode was reasonable (Figure S4C). For docking with F2.I, multiple varied interaction modes were observed (Figure S4D). We checked all the models and chose the most commonly observed hB9L9.3-FZD7^{CRD} model, which also had a larger buried surface and better shape complementarity, for subsequent studies (Figure S4C). On the basis of this docking

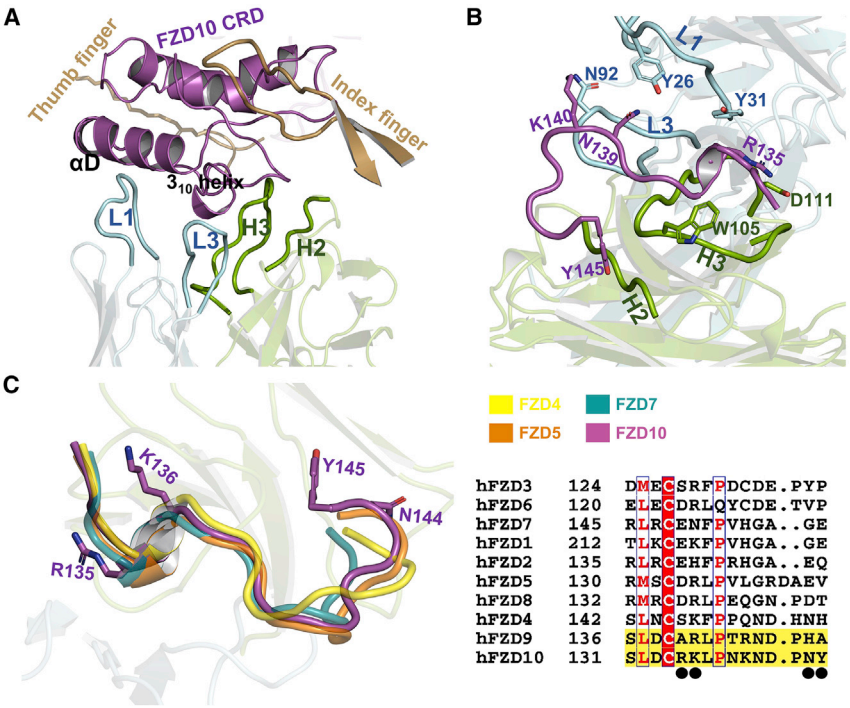

Figure 2. The nonconserved epitope targeted by the FZD10-specific antibody

(A) Position of the epitope targeted by hB9L9.3. The "thumb finger" and "index finger" of XWnt8 are included for localization comparison after superposition of XWnt8-mFZD8^{CRD} (PDB: 4F0A) with FZD10.

(B) Conformation of the FZD10 motif (magenta) and associated CDRs of hB9L9.3 (cyan for light chain and green for heavy chain). Several key residues from the interface are highlighted as sticks.

(C) Structural and sequence comparison of the hB9L9.3 targeting region in different FZDs. The four FZD10-specific residues are shown as sticks in the structure (left) and indicated with black circles in the sequence alignment (right).

See also Figure S3.

model, LCDR3 and HCDR3 were engaged in a shallow groove located around the site II region (Figure 3A). Therefore, we introduced small amino acid compositions at the corresponding positions in the CDRs. For the positions without obviously required preference, we used full amino acid convergence.

Next, we thought that even though the library was designed with site II preference, it should still contain binders recognizing the undesired regions, and these binders could cause screening bias, increasing the difficulty of sorting out the desired target. To solve this problem, we envisioned that preclearing the library with a "counter" antigen sharing all available epitopes except the target epitope as the "positive" antigen would be an effective strategy (Figure 3B). To this end, we designed "counter" antigens by introducing mutations to the site II region on the basis of the docking model (Figure 3C). Two sets of mutations were tested, and one of the resultant proteins, F7M1, retained robust F2.I binding ability (Figure 3D), indicating that it should maintain the native feature for the remaining epitopes and thus fit for removing the unwanted binders. We then conducted the biopanning process as shown in Figure 3E, and after five rounds of selection, we obtained one clone, named pF7_A5, which could bind FZD1/2/7 but not other FZDs (Figure 3F).

According to the binding behavior in the ELISAs (Figure 3F), the epitope targeted by pF7_A5 can distinguish FZD1/2/7 from 10 FZDs but cannot discriminate each member within this subfamily. To verify whether pF7_A5 binds at the site II region, we solved the complex structure of pF7_A5-FZD2^{CRD} (Table 1). The determined structure revealed that pF7_A5 indeed bound FZD2 at the site II region (Figure 3G). Although LCDR1 maintained the predicted configuration, LCDR3 and HCDR3 resided in different positions, changing from the "flat" conformations in the docking model to the "lift-up" conformations in pF7_A5 (Figure 3G). However, even though FZD7 was held at a different position in the pF7_A5-bound structure compared with the docking model, it was still captured by LCDR1, LCDR3, and HCDR3 in a way similar to that in the predicted model (Figure 3G). Together, these results confirmed that by using a directed designed library and "counter" selection strategy, we can successfully identify antibodies binding to the desired epitope.

Structure-guided tuning of pF7_A5 affinity and specificity

As mentioned above, the CD-loop and CT-loop are the structural elements recognized by pF7_A5, and they are grasped on both sides by the clip-like LCDR1 and HCDR3 of pF7_A5 (Figure 3G). Interestingly, HCDR3 folds into an antiparallel β-sheet and packs against the hydrophobic patch of site II (Figure 4A), closely resembling the mode of the hWnt3 index finger interacting with the equivalent region on FZD8.[26] Whether such a "β-sheet covering mode" is generally required for associating with site II remains unknown, but it probably provides an efficient way to interact with a hydrophobic patch. Overlaying FZD5/7/10 onto FZD2 shows that only the CD-loop and CT-loop from FZD7 share almost identical amino acid compositions as well as trajectories as those in FZD2 (Figure 4B), correlating well with the specificity profile of pF7_A5 (Figure 3F).

Guided by the structural information, we next tried to construct a second-generation library to first investigate whether monospecific binders could be identified and second to improve the affinity of pF7_A5. Comparison of site II from FZD2 and FZD7 revealed that only three residues were not conserved (Figures 4B and S5A): H140, E147, and Q148. As a result, we introduced complete randomizations for the corresponding contacting residues in pF7_A5: Y27 and R28 from LCDR1 and L95 from LCDR3 (Figure S5A). In addition, several additional positions located within the interface were also limitedly randomized to further tune the specificity and improve the affinity (Figure S5A). To select the high-affinity variants, the typical strategy of applying increasing stringency was employed (Figure S5B). For selection of

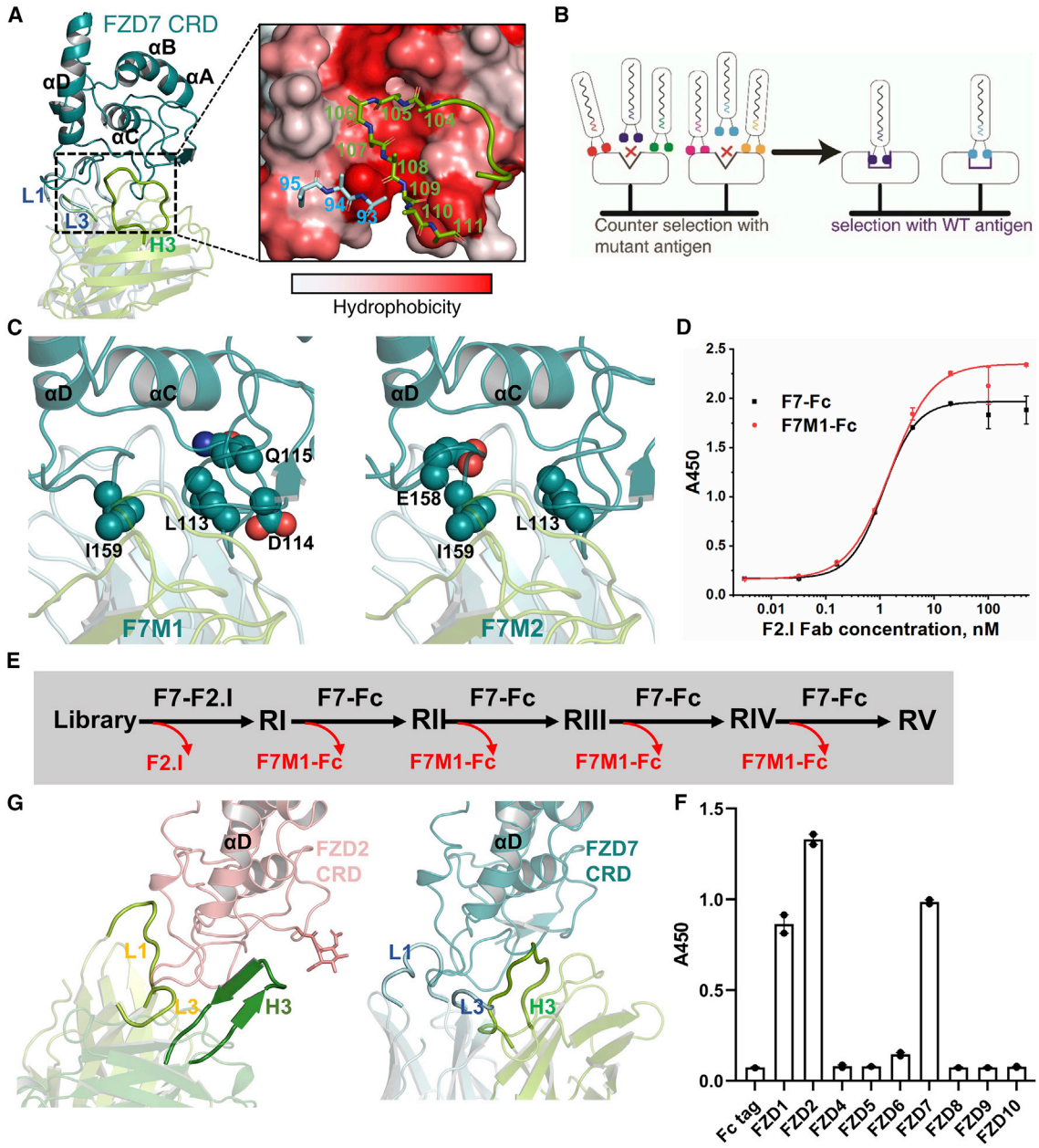

Figure 3. Identification of pF7_A5 with the directed designed library and antigen

(A) LCDR3 and HCDR3 design on the basis of the docking model. The highlighted residues shown as sticks in the close-up view are randomized into small amino acids. The color of the surfaces represents the level of hydrophobicity.

(B) The overall counter selection strategy. The counter antigen will absorb phages displaying undesired antibodies, while the positive antigen enriches target phages.

(C) Counter antigen containing the mutations. Four residues shown as spheres were mutated to alanine in F7M1 (left), and three residues shown as spheres were mutated to alanine in F7M2 (right).

(D) Validation of the folding of F7M1. ELISA of F2.I binding to wild-type FZD7 and F7M1. Fc-tagged proteins were used.

(E) Selection strategy for the five rounds. The counter antigen used in each round is indicated in red.

(F) ELISA results of pF7_A5 (10 nM) binding to FZD proteins. For (D) and (F), data are presented as mean ± SE of two replicates.

(G) Mode of pF7_A5 interacting with FZD2 CRD. The docking model of the antibody complexed with FZD7 CRD (right) is presented for comparison in a similar view. See also Figure S4.

monospecific binders, the "counter" antigen strategy was again used: FZD7 was the "counter" antigen for FZD2 and vice versa (Figure S5B).

After four rounds of affinity-improving selection, we obtained one antibody, termed pF7_B6, which displayed a subnanomolar affinity for FZD7 (Figures S6C). As expected, pF7_B6 lacked

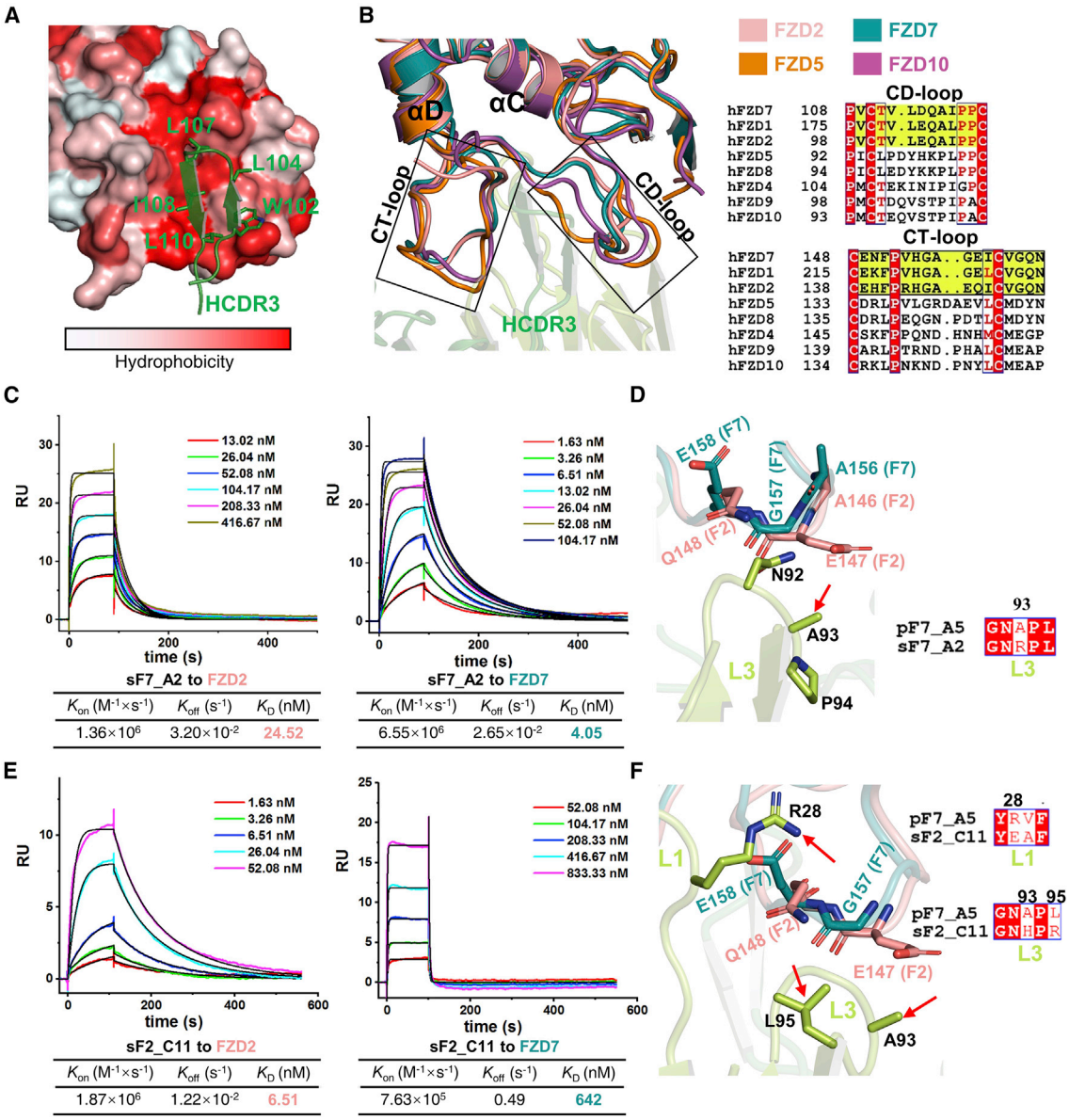

Figure 4. Affinity and specificity tuning of pF7_A5

(A) FZD2 interactions mediated by HCDR3 of pF7_A5. FZD2 is shown as the surface mode, and the color of the surfaces represents the level of hydrophobicity. Key HCDR3 residues (green) are shown as sticks.

(B) Structural (left) and sequence (right) comparison of the CD-loop and CT-loop in different FZDs. The FZD1/2/7 subfamily is highlighted with a yellow background in the sequence alignment.

(C) SPR sensogram data of sF7_A2 binding to FZD2 and FZD7. The solid black lines represent the "1:1 binding" model fits.

(D) Localization of the converted residues of sF7_A2 in the structure. The pF7_A5-FZD2^{CRD} structure was used to map the position of the varied residues.

(E) SPR sensogram data of sF2_C11 binding to FZD2 and FZD7. The solid black lines represent the "1:1 binding" model fits.

(F) Localization of the converted residues of sF2_C11 in the structure. The pF7_A5-FZD2^{CRD} structure was used to map the position of the varied residues.

See also Figures S5 and S6.

specificity and bound FZD1 and FZD2 with nanomolar/subnanomolar affinity (Figures S6A–S6C). For the specificity evolution, no candidate with particular specificity for FZD7 was recovered. The best one, termed sF7_A2, exhibited an approximately 6-fold FZD7 binding preference over FZD2 (Figure 4C). Analysis of the converted residues revealed that the R93 substitution in LCDR3 was suitable for packing with G157 in FZD7 but less favorable for the equivalent E147 in FZD2 (Figure 4D). In contrast to the limited selectivity of sF7_A2, FZD2 selection yielded one highly specific antibody, termed sF2_C11, and it bound FZD2 with a K_d of 6.5 nM, approximately 100-fold smaller than that with FZD7 (Figure 4E). Mapping of the converted residues onto the structure revealed that E28, H93, and R95 in sF2_C11 surrounded the nonconserved FZD2 residues E147 and Q148 and

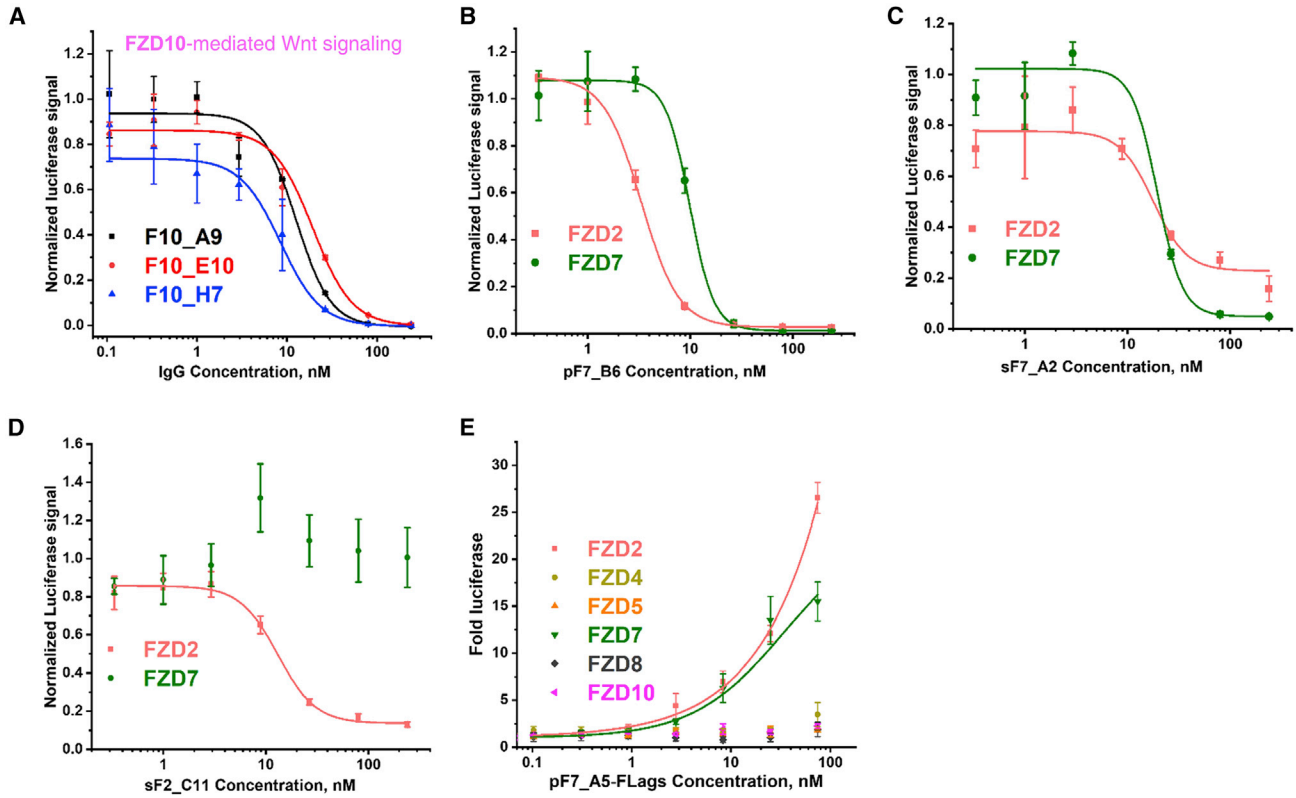

Figure 5. Modulation of the Wnt pathway with the identified antibodies

(A–D) (A) The inhibitory activity of FZD10 antibodies F10_A9, F10_E10, and F10_H7 on the FZD10-mediated Wnt signaling pathway. The inhibitory activity of the high-affinity FZD2/7 antibodies pF7_B6 (B), sF7_A2 (C), and sF2_C11 (D) on the FZD2- or FZD7-mediated Wnt signaling pathway. Cells expressing different FZD receptors were stimulated with 50% Wnt-3A conditioned medium and treated with gradient concentrations of antibodies. The ratios of firefly luminescence to *Renilla* luminescence were calculated, background-subtracted (in reference to samples not stimulated with Wnt3A) and normalized to control samples that were treated with Wnt3A only. The normalized signaling is shown on the y axis.

(E) The activating activity of pF7_A5 FLAg toward different FZD cell lines. For panel E, cells expressing different FZD receptors were treated with gradient concentrations of pF7_A5 FLAgs. The y axis shows the luciferase signal relative to the signal in the absence of any agonist. Data are presented as mean ± SE of at least three replicates.

See also Figure S7

probably produced a complementary shape as well as a polar interaction network with FZD2 (Figure 4F). However, this complementarity would be disrupted by the equivalent G157 and E158 substitution in FZD7, resulting in the lower affinity for FZD7 (Figure 4E). To verify this specificity determinant, we converted G157 and E158 of FZD7 into the corresponding FZD2 residues, and the resultant protein ($FZD7^{G157E/E158Q}$) indeed presented a much higher affinity for sF2_C11 (Figures 4E and S6F). Together, FZD7-preferred and FZD2-specific antibodies were identified by the combinatorial use of a structure-guided library and a natural "counter" antigen of FZD2/FZD7.

WNT SIGNALING MODULATION BY FZD SUBTYPE-SELECTIVE ANTIBODIES

On the basis of the specificity of each antibody toward FZDs, we next evaluated their ability to modulate the cognate signaling pathway in cells. We first generated an F127-knockout (KO) cell line as previously described[33] and verified that the activation of the individual exogenously transfected receptors could be monitored in these cells (Figure S7A). As mentioned above, all FZD10 antibodies, F10_A9, F10_E10, and F10_H7, are site I binders and should antagonize Wnt signal transduction by preventing Wnt binding to FZDs. As expected, F10_A9, F10_E10, and F10_H7 could effectively inhibited the beta-catenin-dependent signaling mediated by FZD10 (Figure 5A). Meanwhile, F10_A9 could partially inhibit FZD5/8-mediated Wnt signaling (Figures S7E and S7F) but not other FZDs, and F10_E10/F10_H7 could not block FZD2/4/5/7/8-mediated Wnt signaling (Figures S7B–S7F), which correlated well with their FZD binding profile (Figure 1A). The FZD2/7 antibodies also exhibited the expected inhibition profiles (Figures 5B–5D and S7D–S7G). Among them, the high-affinity FZD2/7 cross-reactive antibody variant pF7_B6 blocks both FZD2- and FZD7-mediated beta-catenin-dependent signaling with slightly higher potency for the former (Figure 5B). In contrast, sF7_A2 presents higher inhibition efficacy toward FZD7-mediated signaling (Figure 5C), correlating well with its FZD7 binding preference (Figure 4C). Similarly, the FZD2-specific antibody sF2_C11 only inhibited FZD2-mediated signaling (Figure 5D).

In addition to the potential in cancer therapy through antagonizing the Wnt signaling pathway, FZD antibodies also hold

promise for curing degenerative diseases by activating the pathway, as they could be converted into agonists by integrating into FLAgs (Frizzled and LRP5/6 agonists).[34] We then tested the agonistic activity of pF7_A5 in the FLAg form. As expected, pF7_A5 FLAg could activate both the FZD2- and FZD7-mediated beta-catenin-dependent signaling pathways but not others (Figure 5E). The lower potency for the FZD7 pathway is probably due to the relatively lower affinity of pF7_A5 for FZD7 (Figures S7H and S7I). Together, we demonstrated that the identified antibodies could execute specific antagonistic or agonistic modulation of the Wnt signaling pathway.

DISCUSSION

To date, developing effective antibody drugs remains challenging, and one of the reasons is the indeterminacy of the targeting region of these antibodies under development. Accordingly, integrating epitope information into the selection process would greatly increase the success rate. Here, we developed an epitope-directed antibody isolation method by incorporating both directed library design and antigen design. Briefly, the desired region was first set as the contact site with the scaffold antibody for docking analysis, and on the basis of the resultant model, an antibody library favoring the target epitope was designed with human intelligence. This is different from the previously proposed computational approach where sequence design completely relied on computers or the photocrosslinking approach where unbiased libraries were used.[12] In addition to the directed library, a precise "counter" antigen was designed and used in our system to remove irrelevant binders from the library, thus promoting the enrichment of the target antibody. Because of the use of the designed library and antigen, our method can not only fulfill the goal of isolating target epitope binders, as the previously proposed approaches did but also presents additional advantages, for example, allowing affinity as a driving factor for enriching the candidate (Figure 3B). Of note, although the FZD10 library was built on the basis of a "homolog" antibody, using a scaffold antibody recognizing an original site without obvious similarity with the target epitope still succeeded in the case of FZD7, suggesting that this method should be applicable for a broad range of antigens without pre-identified antibodies or homologous antibodies. In this respect, our method is in common with the means involved in *de novo* design by starting with an irrelevant antibody.[11] Furthermore, the relevant concept in the current method can be easily integrated into other antibody identification platforms, such as hybridoma technology. Monoclonal antibodies derived from clonal hybridoma could be tested for binding to both the wild-type (WT) antigen and site-specific mutant, and those showing strong binding signals for the WT antigen rather than the mutant could be ideal candidates. As a result, antibodies possessing the required activities could be sorted out at the early stage, facilitating further affinity optimization and developability tests.

Wnt signaling plays an important role in developmental biology and stem cell maintenance[14]; however, the genetic redundancy of *Wnt* and *FZD* genes, as well as the promiscuous Wnt-FZD interaction, have impeded elucidation of the functional role of individual FZDs in those processes.[35] Using specific tools to modulate the activity of the cognate receptor would be an effective way to solve this problem. Therefore, developing FZD-selective antibodies will not only have clinical significance in established FZD-related cancer therapy but will also help clarify the determinant role of individual FZDs *in vivo*. Attempts have been constantly made using the antibody, peptide, and synthetic scaffold DARPins.[31,36] However, although some have achieved subfamily discrimination, none of the rationally designed modalities accomplishes strict subtype specificity. For example, a selective peptide inhibitor that recognizes FZD1/2/7,[36] DRPB_Fz8 binds specifically to FZD5/8, and DRPB_Fz7 binds to FZD1/2/7.[31] The main reason is that all these binders target site I or nearby regions on CRDs; as a result, it is difficult for them to discriminate each member within the subfamily. In contrast to the conserved feature of site I, the site II region displays more variations and thus could serve as the discriminable epitope for identifying FZD subtype-selective antibodies. Therefore, we set site II as the target epitope and applied the epitope-directed method to develop FZD2/7-selective antibodies. After two generations of design and selection, we identified an FZD2-specific antibody sF2_C11. For FZD7, we obtained the FZD7-preferred antibody sF7_A2. The reason may be because the current library design was more fit for the varied residues of FZD2 but not for those of FZD7. We believe that further evolution on the basis of sF7_A2 could yield an FZD7 exclusive antibody. Altogether, we established an epitope-directed antibody identification method with which several FZD subtype-selective antibodies were derived, providing potential tools for specific Wnt pathway modulation.

STAR★METHODS

Detailed methods are provided in the online version of this paper and include the following:

- KEY RESOURCES TABLE
- RESOURCE AVAILABILITY
  - Lead contact
  - Materials availability
  - Data and code availability
- EXPERIMENTAL MODEL AND SUBJECT DETAILS
- METHOD DETAILS
  - Protein constructs, expression, and purification
  - Docking and directed library design
  - Directed phage display library construction
  - Phage selection against FZD CRDs
  - Enzyme-linked immunosorbent assay
  - Surface plasmon resonance
  - Crystallization and structure determination of Fab-FZD^{CRD} complexes
  - Generation of the F127-KO cell line
  - FZD-specific modulation using luciferase assay
- QUANTIFICATION AND STATISTICAL ANALYSIS

SUPPLEMENTAL INFORMATION

Supplemental information can be found online at https://doi.org/10.1016/j.isci.2022.105636.

ACKNOWLEDGMENTS

We thank staff members at Shanghai Synchrotron Radiation Facility for assistance in data collection. We thank professor Linzhao Cheng's lab for providing the L Wnt-3a cell line. This work was supported by National Key Research and Development Program of China grants 2018YFA0902700 (to Y.T.) and 2017YFA0503600 (to M.T.) and Chinese National Natural Science Foundation grants 31770895 (to Y.T.) and U1732114 (to X.L.).

AUTHOR CONTRIBUTIONS

Q. Ge and Q. Guo designed and constructed the directed libraries, performed phage biopanning, carried out protein purification and binding assays, and helped with manuscript preparation. Q. Ge carried out crystallography and structure determination and analyzed the structure. Q. Ge constructed the KO cell line and performed the luciferase assay. M.T., X.L., and Y.T. designed the overall project. Y.T. supervised the research and wrote the manuscript with input from all authors.

DECLARATION OF INTERESTS

The authors have filed a provisional patent application for the antibodies described in this work.

Received: April 1, 2022
Revised: September 27, 2022
Accepted: November 17, 2022
Published: December 12, 2022

REFERENCES

1. Elgundi, Z., Reslan, M., Cruz, E., Sifniotis, V., and Kayser, V. (2017). The state-of-play and future of antibody therapeutics. Adv. Drug Deliv. Rev. *122*, 2–19. https://doi.org/10.1016/j.addr.2016.11.004.
2. Ribas, A., and Wolchok, J.D. (2018). Cancer immunotherapy using checkpoint blockade. Science *359*, 1350–1355. https://doi.org/10.1126/science.aar4060.
3. Lu, R.M., Hwang, Y.C., Liu, I.J., Lee, C.C., Tsai, H.Z., Li, H.J., and Wu, H.C. (2020). Development of therapeutic antibodies for the treatment of diseases. J. Biomed. Sci. *27*, 1. https://doi.org/10.1186/s12929-019-0592-z.
4. Parray, H.A., Shukla, S., Samal, S., Shrivastava, T., Ahmed, S., Sharma, C., and Kumar, R. (2020). Hybridoma technology a versatile method for isolation of monoclonal antibodies, its applicability across species, limitations, advancement and future perspectives. Int. Immunopharmacol. *85*, 106639. https://doi.org/10.1016/j.intimp.2020.106639.
5. Rajan, S., and Dall'Acqua, W.F. (2020). Emerging strategies for therapeutic antibody discovery from human B cells. In Single-cell Sequencing and Methylation: Methods and Clinical Applications, B. Yu, J. Zhang, Y. Zeng, L. Li, and X. Wang, eds. (Springer Singapore), pp. 221–230. https://doi.org/10.1007/978-981-15-4494-1_18.
6. Pansri, P., Jaruseranee, N., Rangnoi, K., Kristensen, P., and Yamabhai, M. (2009). A compact phage display human scFv library for selection of antibodies to a wide variety of antigens. BMC Biotechnol. *9*, 6. https://doi.org/10.1186/1472-6750-9-6.
7. Persson, H., Ye, W., Wernimont, A., Adams, J.J., Koide, A., Koide, S., Lam, R., and Sidhu, S.S. (2013). CDR-H3 diversity is not required for antigen recognition by synthetic antibodies. J. Mol. Biol. *425*, 803–811. https://doi.org/10.1016/j.jmb.2012.11.037.
8. Frenzel, A., Schirrmann, T., and Hust, M. (2016). Phage display-derived human antibodies in clinical development and therapy. mAbs *8*, 1177–1194. https://doi.org/10.1080/19420862.2016.1212149.
9. Rojas, G., Tundidor, Y., and Infante, Y.C. (2014). High throughput functional epitope mapping: revisiting phage display platform to scan target antigen surface. mAbs *6*, 1368–1376. https://doi.org/10.4161/mabs.36144.
10. Nowak, M.A., May, R.M., Phillips, R.E., Rowland-Jones, S., Lalloo, D.G., McAdam, S., Klenerman, P., Köppe, B., Sigmund, K., Bangham, C.R., and McMichael, A.J. (1995). Antigenic oscillations and shifting immunodominance in HIV-1 infections. Nature *375*, 606–611. https://doi.org/10.1038/375606a0.
11. Nimrod, G., Fischman, S., Austin, M., Herman, A., Keyes, F., Leiderman, O., Hargreaves, D., Strajbl, M., Breed, J., Klompus, S., et al. (2018). Computational design of epitope-specific functional antibodies. Cell Rep. *25*, 2121–2131.e5. https://doi.org/10.1016/j.celrep.2018.10.081.
12. Chen, L., Zhu, C., Guo, H., Li, R., Zhang, L., Xing, Z., Song, Y., Zhang, Z., Wang, F., Liu, X., et al. (2020). Epitope-directed antibody selection by site-specific photocrosslinking. Sci. Adv. *6*, eaaz7825. https://doi.org/10.1126/sciadv.aaz7825.
13. Clevers, H., Loh, K.M., and Nusse, R. (2014). An integral program for tissue renewal and regeneration: Wnt signaling and stem cell control. Science *346*, 1248012. https://doi.org/10.1126/science.1248012.
14. Clara, J.A., Monge, C., Yang, Y., and Takebe, N. (2020). Targeting signalling pathways and the immune microenvironment of cancer stem cells - a clinical update. Nat. Rev. Clin. Oncol. *17*, 204–232. https://doi.org/10.1038/s41571-019-0293-2.
15. Anastas, J.N., and Moon, R.T. (2013). WNT signalling pathways as therapeutic targets in cancer. Nat. Rev. Cancer *13*, 11–26. https://doi.org/10.1038/nrc3419.
16. Gujral, T.S., Chan, M., Peshkin, L., Sorger, P.K., Kirschner, M.W., and MacBeath, G. (2014). A noncanonical Frizzled2 pathway regulates epithelial-mesenchymal transition and metastasis. Cell *159*, 844–856. https://doi.org/10.1016/j.cell.2014.10.032.
17. Steinhart, Z., Pavlovic, Z., Chandrashekhar, M., Hart, T., Wang, X., Zhang, X., Robitaille, M., Brown, K.R., Jaksani, S., Overmeer, R., et al. (2017). Genome-wide CRISPR screens reveal a Wnt–FZD5 signaling circuit as a druggable vulnerability of RNF43-mutant pancreatic tumors. Nat. Med. *23*, 60–68. https://doi.org/10.1038/nm.4219.
18. Merle, P., de la Monte, S., Kim, M., Herrmann, M., Tanaka, S., Von Dem Bussche, A., Kew, M.C., Trepo, C., and Wands, J.R. (2004). Functional consequences of frizzled-7 receptor overexpression in human hepatocellular carcinoma. Gastroenterology *127*, 1110–1122. https://doi.org/10.1053/j.gastro.2004.07.009.
19. Kim, M., Lee, H.C., Tsedensodnom, O., Hartley, R., Lim, Y.-S., Yu, E., Merle, P., and Wands, J.R. (2008). Functional interaction between Wnt3 and Frizzled-7 leads to activation of the Wnt/β-catenin signaling pathway in hepatocellular carcinoma cells. J. Hepatol. *48*, 780–791. https://doi.org/10.1016/j.jhep.2007.12.020.
20. Vincan, E., Darcy, P.K., Farrelly, C.A., Faux, M.C., Brabletz, T., and Ramsay, R.G. (2007). Frizzled-7 dictates three-dimensional organization of colorectal cancer cell carcinoids. Oncogene *26*, 2340–2352. https://doi.org/10.1038/sj.onc.1210026.
21. Yang, L., Wu, X., Wang, Y., Zhang, K., Wu, J., Yuan, Y.C., Deng, X., Chen, L., Kim, C.C.H., Lau, S., et al. (2011). FZD7 has a critical role in cell proliferation in triple negative breast cancer. Oncogene *30*, 4437–4446. https://doi.org/10.1038/onc.2011.145.
22. Nagayama, S., Yamada, E., Kohno, Y., Aoyama, T., Fukukawa, C., Kubo, H., Watanabe, G., Katagiri, T., Nakamura, Y., Sakai, Y., and Toguchida, J. (2009). Inverse correlation of the up-regulation of FZD10 expression and the activation of β-catenin in synchronous colorectal tumors. Cancer Sci. *100*, 405–412. https://doi.org/10.1111/j.1349-7006.2008.01052.x.
23. Nagayama, S., Fukukawa, C., Katagiri, T., Okamoto, T., Aoyama, T., Oyaizu, N., Imamura, M., Toguchida, J., and Nakamura, Y. (2005). Therapeutic potential of antibodies against FZD10, a cell-surface protein, for synovial sarcomas. Oncogene *24*, 6201–6212. https://doi.org/10.1038/sj.onc.1208780.
24. Diamond, J.R., Becerra, C., Richards, D., Mita, A., Osborne, C., O'Shaughnessy, J., Zhang, C., Henner, R., Kapoun, A.M., Xu, L., et al. (2020). Phase Ib clinical trial of the anti-frizzled antibody vantictumab (OMP-18R5) plus paclitaxel in patients with locally advanced or metastatic HER2-negative breast cancer. Breast Cancer Res. Treat. *184*, 53–62. https://doi.org/10.1007/s10549-020-05817-w.

25. Janda, C.Y., Waghray, D., Levin, A.M., Thomas, C., and Garcia, K.C. (2012). Structural basis of Wnt recognition by frizzled. Science *337*, 59–64. https://doi.org/10.1126/science.1222879.

26. Hirai, H., Matoba, K., Mihara, E., Arimori, T., and Takagi, J. (2019). Crystal structure of a mammalian Wnt–frizzled complex. Nat. Struct. Mol. Biol. *26*, 372–379. https://doi.org/10.1038/s41594-019-0216-z.

27. Gurney, A., Axelrod, F., Bond, C.J., Cain, J., Chartier, C., Donigan, L., Fischer, M., Chaudhari, A., Ji, M., Kapoun, A.M., et al. (2012). Wnt pathway inhibition via the targeting of Frizzled receptors results in decreased growth and tumorigenicity of human tumors. Proc. Natl. Acad. Sci. USA *109*, 11717–11722. https://doi.org/10.1073/pnas.1120068109.

28. Raman, S., Beilschmidt, M., To, M., Lin, K., Lui, F., Jmeian, Y., Ng, M., Fernandez, M., Fu, Y., Mascall, K., et al. (2019). Structure-guided design fine-tunes pharmacokinetics, tolerability, and antitumor profile of multi-specific frizzled antibodies. Proc. Natl. Acad. Sci. USA *116*, 6812–6817. https://doi.org/10.1073/pnas.1817246116.

29. Pavlovic, Z., Adams, J.J., Blazer, L.L., Gakhal, A.K., Jarvik, N., Steinhart, Z., Robitaille, M., Mascall, K., Pan, J., Angers, S., et al. (2018). A synthetic anti-Frizzled antibody engineered for broadened specificity exhibits enhanced anti-tumor properties. mAbs *10*, 1157–1167. https://doi.org/10.1080/19420862.2018.1515565.

30. Nakatsuru, S., Katagiri, T., Nakamura, Y., and Endo, K. (2006). TUMOR-TARGETING monoclonal antibodies to FZD10 and uses thereof. Patent Application CA20062655289, 2006/08/24/Application Date.

31. Dang, L.T., Miao, Y., Ha, A., Yuki, K., Park, K., Janda, C.Y., Jude, K.M., Mohan, K., Ha, N., Vallon, M., et al. (2019). Receptor subtype discrimination using extensive shape complementary designed interfaces. Nat. Struct. Mol. Biol. *26*, 407–414. https://doi.org/10.1038/s41594-019-0224-z.

32. Janda, C.Y., Dang, L.T., You, C., Chang, J., de Lau, W., Zhong, Z.A., Yan, K.S., Marecic, O., Siepe, D., Li, X., et al. (2017). Surrogate Wnt agonists that phenocopy canonical Wnt and beta-catenin signalling. Nature *545*, 234–237. https://doi.org/10.1038/nature22306.

33. Voloshanenko, O., Gmach, P., Winter, J., Kranz, D., and Boutros, M. (2017). Mapping of Wnt-Frizzled interactions by multiplex CRISPR targeting of receptor gene families. Faseb. J. *31*, 4832–4844. https://doi.org/10.1096/fj.201700144R.

34. Tao, Y., Mis, M., Blazer, L., Ustav, M., Jr., Steinhart, Z., Chidiac, R., Kubarakos, E., O'Brien, S., Wang, X., Jarvik, N., et al. (2019). Tailored tetravalent antibodies potently and specifically activate Wnt/Frizzled pathways in cells, organoids and mice. Elife *8*, e46134. https://doi.org/10.7554/eLife.46134.

35. Nusse, R., and Clevers, H. (2017). Wnt/beta-Catenin signaling, disease, and emerging therapeutic modalities. Cell *169*, 985–999. https://doi.org/10.1016/j.cell.2017.05.016.

36. Nile, A.H., de Sousa E Melo, F., Mukund, S., Piskol, R., Hansen, S., Zhou, L., Zhang, Y., Fu, Y., Gogol, E.B., Kömüves, L.G., et al. (2018). A selective peptide inhibitor of Frizzled 7 receptors disrupts intestinal stem cells. Nat. Chem. Biol. *14*, 582–590. https://doi.org/10.1038/s41589-018-0035-2.

37. Tiller, T., Meffre, E., Yurasov, S., Tsuiji, M., Nussenzweig, M.C., and Wardemann, H. (2008). Efficient generation of monoclonal antibodies from single human B cells by single cell RT-PCR and expression vector cloning. J. Immunol. Methods *329*, 112–124. https://doi.org/10.1016/j.jim.2007.09.017.

38. Jumper, J., Evans, R., Pritzel, A., Green, T., Figurnov, M., Ronneberger, O., Tunyasuvunakool, K., Bates, R., Žídek, A., Potapenko, A., et al. (2021). Highly accurate protein structure prediction with AlphaFold. Nature *596*, 583–589. https://doi.org/10.1038/s41586-021-03819-2.

39. Varadi, M., Anyango, S., Deshpande, M., Nair, S., Natassia, C., Yordanova, G., Yuan, D., Stroe, O., Wood, G., Laydon, A., et al. (2022). AlphaFold Protein Structure Database: massively expanding the structural coverage of protein-sequence space with high-accuracy models. Nucleic Acids Res. *50*, D439–D444. https://doi.org/10.1093/nar/gkab1061.

40. Honorato, R.V., Koukos, P.I., Jiménez-García, B., Tsaregorodtsev, A., Verlato, M., Giachetti, A., Rosato, A., and Bonvin, A.M.J.J. (2021). Structural biology in the clouds: the WeNMR-EOSC ecosystem. Front. Mol. Biosci. *8*, 729513. https://doi.org/10.3389/fmolb.2021.729513.

41. Dominguez, C., Boelens, R., and Bonvin, A.M.J.J. (2003). HADDOCK: a Protein−Protein docking approach based on biochemical or biophysical information. J. Am. Chem. Soc. *125*, 1731–1737. https://doi.org/10.1021/ja026939x.

42. van Zundert, G.C.P., Rodrigues, J.P.G.L.M., Trellet, M., Schmitz, C., Kastritis, P.L., Karaca, E., Melquiond, A.S.J., van Dijk, M., de Vries, S.J., and Bonvin, A.M.J.J. (2016). The HADDOCK2.2 web server: user-friendly integrative modeling of biomolecular complexes. J. Mol. Biol. *428*, 720–725. https://doi.org/10.1016/j.jmb.2015.09.014.

43. Yan, Y., Tao, H., He, J., and Huang, S.-Y. (2020). The HDOCK server for integrated protein–protein docking. Nat. Protoc. *15*, 1829–1852. https://doi.org/10.1038/s41596-020-0312-x.

44. Nile, A.H., Mukund, S., Stanger, K., Wang, W., and Hannoush, R.N. (2017). Unsaturated fatty acyl recognition by Frizzled receptors mediates dimerization upon Wnt ligand binding. Proc. Natl. Acad. Sci. USA *114*, 4147–4152. https://doi.org/10.1073/pnas.1618293114.

45. Winn, M.D., Ballard, C.C., Cowtan, K.D., Dodson, E.J., Emsley, P., Evans, P.R., Keegan, R.M., Krissinel, E.B., Leslie, A.G.W., McCoy, A., et al. (2011). Overview of the CCP4 suite and current developments. Acta Crystallogr. D Biol. Crystallogr. *67*, 235–242. https://doi.org/10.1107/S0907444910045749.

46. Tonikian, R., Zhang, Y., Boone, C., and Sidhu, S.S. (2007). Identifying specificity profiles for peptide recognition modules from phage-displayed peptide libraries. Nat. Protoc. *2*, 1368–1386. https://doi.org/10.1038/nprot.2007.151.

47. Minor, W., Cymborowski, M., Otwinowski, Z., and Chruszcz, M. (2006). HKL-3000: the integration of data reduction and structure solution - from diffraction images to an initial model in minutes. Acta Crystallogr. D Biol. Crystallogr. *62*, 859–866. https://doi.org/10.1107/S0907444906019949.

48. Adams, P.D., Afonine, P.V., Bunkóczi, G., Chen, V.B., Davis, I.W., Echols, N., Headd, J.J., Hung, L.-W., Kapral, G.J., Grosse-Kunstleve, R.W., et al. (2010). PHENIX: a comprehensive Python-based system for macromolecular structure solution. Acta Crystallogr. D Biol. Crystallogr. *66*, 213–221. https://doi.org/10.1107/S0907444909052925.

49. Chang, T.-H., Hsieh, F.-L., Zebisch, M., Harlos, K., Elegheert, J., and Jones, E.Y. (2015). Structure and functional properties of Norrin mimic Wnt for signalling with Frizzled4, Lrp5/6, and proteoglycan. Elife *4*, e06554. https://doi.org/10.7554/eLife.06554.

50. Chen, P., Tao, L., Wang, T., Zhang, J., He, A., Lam, K.-H., Liu, Z., He, X., Perry, K., Dong, M., and Jin, R. (2018). Structural basis for recognition of frizzled proteins by Clostridium difficile toxin B. Science (New York, N.Y.) *360*, 664–669. https://doi.org/10.1126/science.aar1999.

51. Strong, R.K., Campbell, R., Rose, D.R., Petsko, G.A., Sharon, J., and Margolies, M.N. (1991). Three-dimensional structure of murine anti-p-azophenylarsonate Fab 36-71. 1. X-ray crystallography, site-directed mutagenesis, and modeling of the complex with hapten. Biochemistry *30*, 3739–3748. https://doi.org/10.1021/bi00229a022.

52. Emsley, P., Lohkamp, B., Scott, W.G., and Cowtan, K. (2010). Features and development of Coot. Acta Crystallogr. D Biol. Crystallogr. *66*, 486–501. https://doi.org/10.1107/S0907444910007493.

53. Schrodinger, L.L.C. (2015). The PyMOL Molecular Graphics System Version 1.8.

STAR★METHODS

KEY RESOURCES TABLE

REAGENT or RESOURCE	SOURCE	IDENTIFIER
Antibodies		
Anti-M13 Antibody (HRP), Mouse Monoclonal	sinobiological	Cat#11973-MM05T-H
Anti-HA tag Antibody (HRP), Mouse Monoclonal	sinobiological	Cat#100028-MM10-H
HRP-conjugated Monoclonal mouse anti-human Ig kappa chain antibody	hepengbio	Cat#C030243
Bacterial and virus strains		
E.coli DH5α	NEB	Cat#C2987H
E.coli XL1-Blue	In house	N/A
E.coli SS320	In house	N/A
Chemicals, peptides, and recombinant proteins		
DMEM	Cytiva	Cat#SH30262.01
FBS	LONSERA	Cat# S711-001S
Penicillin–streptomycin	Cytiva	Cat#SV30010
Union 293 Cell Cuture Medium	Union-Biotech (shanghai) Co., Ltd	Cat#UP1000
PolyJet™ *In Vitro* DNA Transfection Reagent	signagen	Cat#SL100688
PEI	Polysciences, Inc	Cat#24765
Index	Hampton Research	Cat#HR2-144
PEG/Ion Screen I&II	Hampton Research	Cat#HR2-126 & HR2-098
Crystal Screen I&II	Hampton Research	Cat#HR2-110 & HR2-112
ProPlex	Molecular Dimensions	Cat#MD1-38
TMB Substrate	beyotime	Cat#P0209-500
Critical commercial assays		
TransDetect® Double-Luciferase Reporter Assay Kit	TransGen Biotech, Beijing, China	Cat#FR201-02
Deposited data		
Frizzled10 CRD in complex with F10_A9 Fab	This paper	PDB ID: 7X8Q
Frizzled10 CRD in complex with hB9L9.3 Fab	This paper	PDB ID: 7X8T
Frizzled2 CRD in complex with pF7_A5 Fab	This paper	PDB ID: 7X8P
Crystal structure of Frizzled 5 CRD in complex with F2.I Fab	(Raman et al., 2019)	PDB ID: 6O39
Crystal structure of Frizzled 7 CRD	(Nile et al., 2017)	PDB ID: 5T44
Crystal structure of Frizzled 2 CRD in complex with *Clostridium difficile* toxin B	(Chen et al., 2018)	PDB ID: 6C0B
Crystal structure of Frizzled 4 CRD - Crystal Form I	(Chang et al., 2015)	PDB ID: 5BPB
CRYSTAL STRUCTURE OF THE FAB FRAGMENT FROM THE HUMAN MYELOMA IMMUNOGLOBULIN IGG	(Strong et al., 1991)	PDB ID: 8FAB
Crystal structure of XWnt8 in complex with the cysteine-rich domain of Frizzled 8	(Janda et al., 2012)	PDB ID: 4F0A
Crystal structure of a mammalian Wnt-frizzled complex	(Hirai et al., 2019)	PDB ID: 6AHY
Experimental models: Cell lines		
Expi293F™ Cells	Thermo Fisher	Cat#A14527
HEK293T	ATCC	Cat#CRL-3216
L Wnt-3A, a gift from Professor Linzhao Cheng	Procell Life Science&Technology Co.,Ltd.	Cat#CL-0375

(*Continued on next page*)

Continued

REAGENT or RESOURCE	SOURCE	IDENTIFIER
Oligonucleotides		
Primers for FZD1/2/7 KO plasmid I, forward: atttcttggcttta tatatcttgtggaaaggacgaaacaccGGCGATGTCCGTGCACAGC	GenScript	F127KO-I-F
Primers for FZD1/2/7 KO plasmid I, reverse: ggactagccttat tttaacttgctatttctagctctaaaacGCTGTGCACGGACATCGCC	GenScript	F127KO-I-R
Primers for FZD1/2/7 KO plasmid III, forward: tttcttggctttat atatcttgtggaaaggacgaaacaccgATCTCCATCCCGCTGTGCA	GenScript	F127KO-III-F
Primers for FZD1/2/7 KO plasmid III, reverse: gactagccttatt ttaacttgctatttctagctctaaaacTGCACAGCGGGATGGAGATc	GenScript	F127KO-III-R
Primers for directed library construction, see Table S3	GenScript	N/A
Software and algorithms		
HKL3000	(Minor et al., 2006)	https://www.hkl-xray.com/hkl-3000
PHENIX Version 1.20	(Adams et al., 2010)	https://phenix-online.org/
COOT Version 0.8.9.2	(Emsley et al., 2010)	https://www2.mrc-lmb.cam.ac.uk/personal/pemsley/coot/
CCP4 V7.0	(Winn et al., 2011)	https://www.ccp4.ac.uk/
AlphaFold	(Jumper et al., 2021)	https://alphafold.com/
PyMOL(TM) Molecular Graphics System, Version 2.5.0.	Schrödinger, LLC	https://pymol.org/2/
HADDOCK 2.4	(van Zundert et al., 2016)	https://www.bonvinlab.org/software/haddock2.4/
HDOCK	(Yan et al., 2020)	http://hdock.phys.hust.edu.cn/
OriginPro 2018C	originlab	https://www.originlab.com
Biacore T200 Evaluation Software	Cytiva	https://www.cytivalifesciences.com/en/us/support/software/biacore-downloads/biacore-t200-software
Other		
QIAquick PCR Purification Kit	Qiagen	Cat#28104
rProtein A Sepharose Fast Flow	Cytiva	Cat#GE17-1279-01
Ni Sepharose® 6 Fast Flow	Cytiva	Cat# 17531802
Superdex™ 200 Increase 10/300 column	Cytiva	Cat#28990944
Maxisorp immunoplates	Thermo Fisher	Cat#44–2404
Amino acid sequences of the identified antibodies, Table S3	This paper	N/A

RESOURCE AVAILABILITY

Lead contact

Further information and requests for resources and reagents should be directed to and will be fulfilled by the lead contact, Yuyong Tao (taoyy@ustc.edu.cn).

Materials availability

All unique/stable reagents generated in this study are available from the lead contact with a completed Materials Transfer Agreement.

Data and code availability

The atomic coordinates and structure factors for the crystal structures reported in this article have been deposited in the PDB. Accession numbers are listed in the key resources table.

This paper does not report original code.

Any additional information required to reanalyze the data reported in this work paper is available from the lead contact upon request.

EXPERIMENTAL MODEL AND SUBJECT DETAILS

HEK 293T cells and L Wnt-3a cells used for functional assay were maintained at 37°C in a humidified atmosphere comprising 5% CO_2 in Dulbecco's minimal essential medium (DMEM) containing 10% (v/v) heat-inactivated fetal bovine serum (FBS) and 100 U/mL of

penicillin–streptomycin. Expi 293F cells used for protein expression was cultured in Union 293 Cell Cuture Medium (Union-Biotech (shanghai) Co., Ltd) supplemented with 5% CO_2 for maintenance. *Escherichia coli* DH5α used for vector amplification was cultured in LB media with appropriate antibiotics. *Escherichia coli* XL1-blue and *Escherichia coli* SS320 used for phage display were cultured in 2YT medium with appropriate antibiotics.

METHOD DETAILS

Protein constructs, expression, and purification

The genes encoding FZD CRDs, including FZD1 (residues 73–253), FZD2 (residues 29–168), FZD4 (residues 42–164), FZD5 (residues 27–167), FZD6 (residues 19–153), FZD7 (residues 33–165), FZD8 (residues 25–172), FZD9 (residues 23–160), and FZD10 (residues 21–161), were cloned into the pME vector (derived from AbVec2.0-IGHG1)[37] with a N-terminal human trypsinogen-2 signal peptide and a C-terminal Fc tag (hIgG1). Site-directed mutagenesis was performed to generate F7M1 and F7M2 mutants. For full-length IgG, the V_L and V_H domains of the corresponding antibody sequence were obtained by DNA synthesis (for hB9L9.3) or overlap PCR and were further cloned into mammalian expression vectors designed for the production of light chain or IgG1 heavy chain. In addition, an HA epitope tag was attached to the C-terminus of the light chain of hB9L9.3 and pF7_A5 for detection.

All Fc-tagged human FZD CRDs or full-length IgG were expressed by transient transfection in Expi 293F cells (Thermo Fisher) using PEI (Polysciences, Inc). For full-length IgG, the corresponding heavy chain and light chain plasmid pair was cotransfected at a molar ratio of 3:2. The Fc-tagged antigens or antibodies were purified by protein A chromatography from cell culture media. Briefly, the collected supernatant was added with 1/10 supernatant volume of 10×PBS to improve the binding to protein A resin, and was subsequently incubated with protein A resin (Cytiva), which was pre-equilibrated in PBS. After incubating for 2 hours, the resin was washed with 10 column volumes of PBS, then the protein sample bound to the resin was eluted with 10 mL of elution buffer (0.2 M arginine, pH 2.7). Immediately after elution, 1 mL of tris-HCl (1 M, pH 8.0) was added to adjust the pH. The eluted proteins were buffer-exchanged into PBS by spin concentration and stored in aliquots at −80°C.

To prepare F10_A9-FZD10^{CRD} and hB9L9.3-FZD10^{CRD} complexes, FZD10 (residues 24–152 with the N48Q mutation) along with the antibody heavy chain (V_H-C_{H1}, with a C-terminal histidine tag) and light chain were co-transfected into Expi 293F cells (Thermo Fisher) at a ratio of 1.5:1:1. To prepare the pF7_A5-FZD2^{CRD} complex, FZD2 (residues 24–152 with a C-terminal histidine tag) along with the heavy chain and light chain were co-transfected into Expi 293F cells (Thermo Fisher) at a ratio of 1.5:1:1. The antigen-Fab complexes were purified using Ni-NTA affinity chromatography (Cytiva) from cell culture media. Briefly, the collected supernatant was added with 1/10 supernatant volume of buffer A (400 mM NaH_2PO_4, pH 8.0, 1.0 M NaCl), then $CaCl_2$ was added to a final concentration of 2 mM to remove the chelating agents. The supernatant was isolated by centrifugation at 12,000 × g for 30 min and incubated with Ni Sepharose® 6 Fast Flow resin (Cytiva) at 4 °C. After incubating for 2 hours, protein was eluted with elution buffer (20 mM Tris, pH 7.8, 300 mM NaCl, 200 mM imidazole), followed by gel filtration chromatography (Superdex 200 Increase 10/300 column, Cytiva) in 20 mM Tris, pH 7.8 and 100 mM NaCl buffer. The complex fractions were collected and concentrated using a 10-kDa molecular weight cutoff concentrator (Millipore) for crystallization trials.

Docking and directed library design

To obtain the FZD10 site I antibody, the FZD10 CRD model from AlphaFold[38,39] was aligned with F2.I-FZD5^{CRD} crystal structure (PDB: 6O39) and interface design were performed on F2.I to obtain antigen contacting CDR residues (Figure S2B). These residues were fully randomized by introducing degenerate NNK codons.

To obtain the template for the FZD2/7 site II binder, molecular docking was utilized to obtain the original model. F2.I and hB9L9.3 were chosen as the templates for docking against the FZD7 CRD site II region. Before docking, residues at LCDR3, HCDR1, HCDR2, HCDR3 of F2.I and LCDR1, LCDR2, and HCDR3 of hB9L9.3 were manually mutated to alanine to eliminate potential side chain clashes during sampling according to a previous report. The potential binding models were generated by HADDOCK 2.4[40–42] and HDOCK[43] to dock the mutated complementarity determining regions against the site II region of the FZD7 CRD (PDB: 5T44).[44] The cluster with the highest score was examined visually for further analysis. For each docking model, the buried surface area and shape complementarity score were calculated with the AreaIMol and Sc programs from the CCP4 program suite.[45] Based on the docking mode with the hB9L9.3 template, residues 93–95 in the light chain and residues 104–111 in the heavy chain were mutated to small hydrophobic residues; thus, the VBC codon was employed. The remaining residues, including residues 26–31 (LCDR1), residues 49 (LCDR2), residues 91–92 (LCDR3) in the light chain and residues 101–103 (HCDR3) in the heavy chain, were fully randomized by introducing NNK codons.

To fine tune the specificity and binding affinity of pF7_A5, a second-generation library was constructed according to Table S1. In addition, we manually prepared some mutations at residue S31 in the light chain. All the primers designed for directed library construction are listed in Table S2.

Directed phage display library construction

For library construction, a scFV backbone was first constructed by joining the corresponding V_L and V_H regions with an 18-aa linker. Then, according to the desired directed library design, forward and reverse primers (GenScript) containing degenerate codons and flanking regions were annealed to the scFV backbone to initiate PCR. The first round of PCR products was combined by overlapping PCR. The purified PCR products along with the restriction enzyme-digested phagemid vector were integrated by Gibson assembly.

The Gibson reaction products were purified by a QIAquick PCR Purification Kit (QIAGEN) and transformed into *E. coli* SS320 (pre-infected with M13KO7 helper phage) by electroporation. After electroporation, the cells were immediately recovered in SOC media and were further transferred to 2YT medium supplemented with ampicillin and kanamycin for phage propagation.

Phage selection against FZD CRDs

Phage panning was performed according to previously established protocols[46] with some modifications. All antigens for counter selection or positive selection were coated in Maxisorp immunoplates (Thermo Fisher) at 4°C overnight. Then the plates were blocked with 200 μL PBT buffer (PBS containing 0.5% bovine serum albumin and 0.05% Tween-20) for 2 hours at room temperature. For $FZD10^{CRD}$ site I antibody identification, the phage pool was first cleared by incubation with Fc tag proteins for 1 hour. The unbound phage was then incubated with Fc-tagged FZD10 CRD for 1 hour. After washing 10 times with PT buffer (PBS buffer containing 0.05% Tween-20), the bound phage was harvested with 100 mM HCl and then neutralized with Tris-HCl buffer (1 M, pH 11). The eluted phage was used to infect actively growing *E. coli* XL1-Blue cells (OD600<0.8) in 2YT media for propagation. In total, four rounds of biopanning were performed, and individual phage clones from the fourth round of selection were tested by phage ELISA.

For FZD7 site II binder screening, different selection strategies were employed (as shown in Figure 3E). In round I, previously reported F2.I Fab was used to block the site I epitope of the FZD7 CRD. Thus, the F2.I-$FZD7^{CRD}$ complex was used for positive selection, F2.I Fab was used for negative selection. Round II-Round V was performed using F7M1-Fc for counter selection and WT antigen for positive selection. Individual phage clones from the fifth round of selection were tested by phage ELISA.

To obtain FZD2/7 high-affinity and specific antibodies, combinatorial screening strategies were employed (Figure S5B). To obtain high-affinity antibodies, the Fc protein was used for counter selection. In round III and round IV, fewer antigens were coated, and a kinetics selection protocol was used. After counter selection with Fc protein, the phage pool was first incubated with antigens. The unbound phage was washed away with PT buffer. Subsequently, the bound phages were incubated with 1 μM free cognate antigen to remove phages with high K_{off}. To obtain specific antibodies, a counter selection strategy was used. For the FZD2-specific binder, FZD7 was used for counter selection. In round IV, the phage pool was further purified by adding excessive FZD7 CRD for competition. Accordingly, the FZD2 CRD was used for counter selection for FZD7-specific antibody identification. Individual phage clones from the fourth round of selection were tested by phage ELISA. The amino acid sequences of all identified antibodies were summarized in Table S3.

Enzyme-linked immunosorbent assay

Antigen (0.1 μg) in 100 μL of PBS was coated in Maxisorp immunoplates (Thermo Fisher) at 4°C overnight. The plate was blocked with 200 μL PBT buffer (PBS containing 0.5% bovine serum albumin and 0.05% Tween-20) for 2 hours at room temperature. After washing three times with PT buffer, samples (antibodies or phages) diluted in PBT buffer were incubated for 1 hour. For competitive ELISAs, competitors were added and incubated for another 1 hour. Wells were washed five times with 200 μL PT buffer. Subsequently, horseradish peroxidase (HRP)-conjugated secondary antibody was added at a dilution in PBT buffer and incubated for 30 min at room temperature. Wells were then washed seven times with 200 μL PT buffer. Then, 100 μL TMB substrate (Beyotime) was added to each well and incubated for 3 to 10 min. The reaction was quenched by adding 50 μL of 2 M H_2SO_4, and the absorbance at 450 nm was measured using a Synergy H1 microplate reader (BioTek). The data were analyzed by OriginPro (Origin Lab). For phage ELISAs, HRP-conjugated anti-M13 antibody (1:10000, Sino Biological, Inc., Beijing) was used. For binding assays of hB9L9.3 and pF7_A5, HRP-conjugated anti-HA tag antibody (1:5000, Sino Biological, Inc., Beijing) was used. For binding assays of F10_A9, F10_E10, F10_H7 and F2. I, HRP-conjugated anti-kappa chain antibody (1:10000, hepengbio) was used.

Surface plasmon resonance

Surface plasmon resonance measurements were performed by a Biacore T200 instrument (Cytiva) with PT buffer as the running buffer. Fc-tagged FZD CRDs (60–100 RUs) were immobilized by amine coupling to a CM5 sensor chip. Analyte proteins serially diluted in PT buffer were subjected to the chip with a flow rate of 30 μL/min. The chip surface was regenerated after each injection with 10 mM NaOH. For binding kinetics, sensorgrams were fitted to a "1:1 binding" binding mode for Fab fragments and to a "bivalent analyte" mode for IgG using Biacore T200 Evaluation Software (Cytiva).

Crystallization and structure determination of Fab-FZD^{CRD} complexes

All the Fab-FZD^{CRD} complexes were set up for crystallization at concentrations of 10–20 mg/mL. Complexes were mixed with conditions from a commercial screening kit (Hampton and Molecular Dimension) at a 1:1 ratio. The F10_A9-$FZD10^{CRD}$ complex crystallized in a condition containing 0.1 M HEPES (pH 7.0), 30% Jeffamine ®ED-2001 (pH 7.0) and diffracted to a resolution of 2.65 Å. The hB9L9.3-$FZD10^{CRD}$ complex crystallized in a condition containing 0.1 M Na citrate (pH 5.0), 15% PEG 8000 and diffracted to a resolution of 2.5 Å. The pF7_A5-$FZD2^{CRD}$ complex crystallized in a condition containing 8% Tacsimate™ (pH 4.0) and 20% PEG 3350 and diffracted to a resolution of 2.25 Å. All the data were collected at the BL18U beamline of Shanghai Synchrotron Radiation Facility. The data were processed and scaled by HEK3000.[47] Structures were determined by molecular replacement using Phaser-MR[48] with FZD4 (PDB ID: 5BPB)[49] or FZD2 (PDB ID: 6C0B)[50] and Fab (PDB ID: 8FAB)[51] as search models. Iterations of model building and refinement were performed using Coot[52] and phenix.refine.[48] Data collection and refinement statistics are summarized in Table 1. The molecular graphic figures were prepared with PyMOL.[53]

Generation of the F127-KO cell line

To investigate Wnt signaling activation mediated by individual FZD receptors, an FZD1/2/7 knockout cell line was constructed using the CRISPR–Cas9 system as previously described.[33] Briefly, oligonucleotides containing sgFZD1,2,7-I (5′- GGCGATGTCCGT GCACAGC-3′) or sgFZD1,2,7-III (5′-gATCTCCATCCCGCTGTGCA-3′) with flanking sequences were annealed and cloned into the BbsI (Thermo Fisher) digested pSpCas9 (BB)-2A-Puro plasmid (PX459; Addgene, Cambridge, MA, USA). HEK293T cells were transiently transfected with the plasmid using Polyjet (Signagen) following the manufacturer's instructions. After 48 h, selection with 2 μg/mL puromycin for 48 h was performed. The cell pools of HEK293T cells were grown for 7 d with 0.5 μg/mL puromycin before experiments.

FZD-specific modulation using luciferase assay

Wnt transcriptional activity was assessed using the TOPflash assay. In brief, 2×10^6 cells were seeded in 6-cm cell culture dishes on the first day. On the second day, the cells were transfected with 1 μg FZD receptor, 950 ng TCF/firefly luciferase reporter and 50 ng *Renilla* luciferase (control reporter) using PolyJet (Signagen) following the manufacturer's instructions. On the third day, the transfected cells were collected and re-plated in 96-well plates (8×10^4 cells per well). For the inhibition assay, the cells were incubated with 50% Wnt3a-CM (generated from L-cells stably expressing Wnt3a) and gradient concentrations of antibodies for 24 h. For the activation assay, the cells were stimulated with gradient concentrations of FLags for 24 h. These cells were washed with PBS buffer and lysed as instructed in the TransDetect® Double-Luciferase Reporter Assay Kit (TransGen Biotech, Beijing, China) user manual. Luminance signals were recorded by a Synergy H1 microplate reader (BioTek). The ratios of firefly luciferase to *Renilla* luciferase were calculated, background-subtracted (in reference to samples not stimulated with Wnt3A) and normalized to control samples that were treated with Wnt3A only.[36] The data were analyzed by OriginPro (Origin Lab). The IC_{50} and inhibition efficacy of all identified antibodies were summarized in Table S4.

QUANTIFICATION AND STATISTICAL ANALYSIS

Average and standard deviation values were determined using AVERAGE and STDEV functions in Microsoft Excel. Sample sizes (n) and data processing details are provided in figure legend. The statistical analysis and data plotting were performed on OriginPro (Origin Lab) and GraphPad Prism software. Details for the statistical analysis of X-ray crystallography data are provided in Table 1.